2014 22nd Mediterranean Conference on Control and Automation (MED)
University of Palermo. June 16-19, 2014. Palermo, Italy

# A Safe Position Tracking Strategy for Multirotor Helicopters

Igor Afonso Acampora Prado, [1], igorap@ita.br
Davi Antônio dos Santos,[1], davists@ita.br
[1] Instituto Tecnológico de Aeronáutica, Sao José dos Campos, Brazil 12228-900

***Abstract*—The interest for multirotor unmanned aerial vehicles (UAVs) is currently growing due to their low cost, high maneuverability, simplified mechanics, capability to perform vertical take-off and landing as well as hovering flight. These characteristics make them a promising technology suitable for applications such as surveillance of indoor environments. The present work faces the problem of safely controlling the position trajectory of multirotor UAVs by taking into consideration a conic constraint on the total thrust vector and a linear convex constraint on the position vector. The problem is solved using a linear state-space model predictive control (MPC) strategy, whose optimization is made handy by replacing the original conic constraint set on the thrust vector by an inscribed pyramidal space, which renders a linear set of inequalities. The control vector computed by the MPC is converted into a throttle command and an attitude command. The proposed method is evaluated on the basis of Monte-Carlo simulations taking into account a random disturbance force. The simulations show the effectiveness of the method in tracking the commanded trajectory while respecting the control and position constraints. They also predict the effect of both the commanded speed and the maximum inclination constraint on the system performance.**

## I. Introduction

The multirotor-type unmanned aerial vehicle (UAV) technology has attracted a great deal of interest of the academia and industry and, consequently experienced a rapid improvement. This interest is justified by features such as their simplified mechanics, low cost, high maneuverability, and vertical take-off and landing (VTOL) capability. Multirotor UAVs have been used both in military and civil activities, focusing on applications too risky to human beings or simply intended to increase the efficiency of certain tasks. Examples of applications are building surveillance [1], traffic monitoring, topological modelling of urban and agriculture areas, delivering and search and rescue [2].

It is well-known that the multirotors have an under-actuated dynamics with six degrees of freedom (DOF) and four independent controls. Namely, they have three DOFs of translation and three DOFs of rotation and can be actuated by three torque components and the magnitude of the total thrust vector. It could seem that a grave difficulty in designing a control system for a multirotor is the need for facing that under-actuation characteristic. However, it is necessary take into consideration that in most of the practical applications, one is indeed interested in controlling at most four DOFs: the three-dimensional position and the heading angle. Figura 1 shows the block diagram of a control system for controlling only the three-dimensional position $\mathbf{r} \in \mathbb{R}^3$ of a multirotor to follow a time-varying position command $\mathbf{r}_\mathrm{d} \in \mathbb{R}^3$. This system is organized in two loops: an inner loop for attitude control and an outer loop for position control. The Navigation System block is responsible for estimating the vehicle's attitude $\mathbf{D} \in \mathrm{SO}(3)$, angular velocity $\boldsymbol{\omega} \in \mathbb{R}^3$, position $\mathbf{r}$, and linear velocity $\dot{\mathbf{r}} \in \mathbb{R}^3$. The Attitude Control block receives an attitude command $\mathbf{D}_\mathrm{d} \in \mathrm{SO}(3)$ and produces the control torque $\boldsymbol{\tau} \in \mathbb{R}^3$ to incline the rotor plane with respect to the horizontal plane as desired. The Position Control block has the role of generating the throttle command (command for the total thrust magnitude) $f \in \mathbb{R}$ and the attitude command $\mathbf{D}_\mathrm{d}$ necessary to accelerate the multirotor in such a way to control its position as desired.

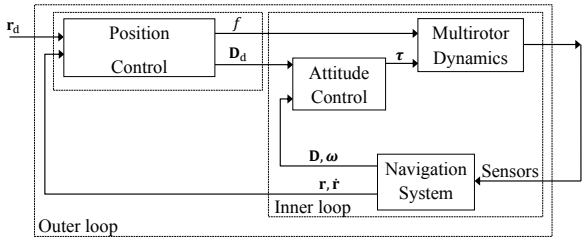


Fig. 1. Block diagram of a multirotor position tracking control system.

The community has made many efforts to devise autonomous control systems for multirotor attitude and position tracking. Reference [3] presents a control law designed on the basis of the feedback linearization technique for guiding a quadrotor through a reference trajectory. [4] applied the nested-saturated controller to the positioning and attitude stabilization. Reference [5] designed two control laws using, respectively, the sliding mode and the backstepping methods; the authors showed by simulations that the backstepping method outperforms the slide mode one. Reference [6] proposed a control system constituted by a model predictive controller (MPC) for position tracking and a nonlinear $\mathrm{H}_\infty$ controller for attitude stabilization under aerodynamic disturbances and parametric as well as structural uncertainties. Reference [7] designed a single MPC controller to reach simultaneous position control and attitude stabilization. None of the aforementioned works

dealt with constraints on the control force. More recently, [9] and [10] tackled the problem of controlling the position of a multirotor while respecting constraints on the inclination of the rotor plane and on the magnitude of the total thrust vector. Reference [9] presented a very simple but effective control method derived using the feedback linearization and a proportional-derivative control law. The reference [10] solved the same problem by using the Retrospective Cost Adaptive Control (RCAC) strategy.

In the present paper, the problem tackled in [9]–[10] is extended to include a linear convex constraint on the position vector. This additional constraint is introduced in order to prevent collisions with walls, the ceiling, and the floor of a box-shaped indoor environment. The problem is solved by a simple linear MPC. As the corresponding thrust constraint set is a piece of a cone with inferior and superior spherical lids, in its original form, it renders a nonlinear and non-convex optimization problem. In order to make the optimization handy, that conic space is replaced by an inscribed rectangular pyramid, yielding a linear convex set of inequality constraints. The remaining text is organized as follows. Section 2 defines a position tracking problem. Section 3 presents a linear MPC to tackle the position tracking problem. Section 4 evaluates the proposed method on the basis of computational simulations. Finally, Section 5 presents the paper's conclusions.

## II. Problem Statement

Consider the multirotor vehicle and the three Cartesian coordinate systems (CCS) illustrated in Figure 2. Assume that the vehicle has a rigid structure. The body CCS $S_{\mathrm{B}} \triangleq \{X_{\mathrm{B}}, Y_{\mathrm{B}}, Z_{\mathrm{B}}\}$ is fixed to the structure and its origin coincides with the center of mass (CM) of the vehicle. The reference CCS $S_{\mathrm{R}} \triangleq \{X_{\mathrm{R}}, Y_{\mathrm{R}}, Z_{\mathrm{R}}\}$ is Earth-fixed and its origin is at point $O$. Finally, the CCS $S_{\mathrm{R}'} \triangleq \{X_{\mathrm{R}'}, Y_{\mathrm{R}'}, Z_{\mathrm{R}'}\}$ is defined to be parallel to $S_{\mathrm{R}}$, but its origin is shifted to CM. Assume that $S_{\mathrm{R}}$ is an inertial frame.

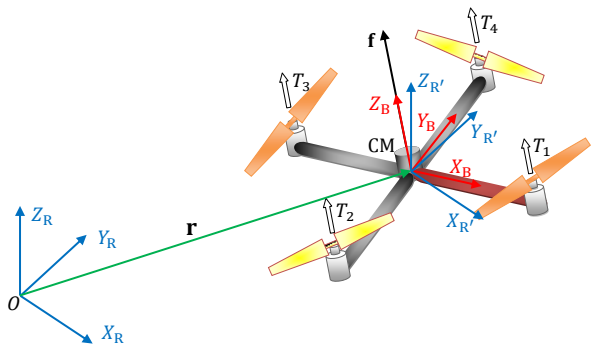


Fig. 2. The Cartesian coordinate systems.

Invoking the second Newton's law and neglecting disturbance forces, the translational dynamics of the multirotor illustrated in Figure 2 can be immediately described in $S_{\mathrm{R}}$ by the following second order differential equation:

$$\ddot{\mathbf{r}} = \frac{1}{m}\mathbf{f} + \begin{bmatrix} 0 \\ 0 \\ -g \end{bmatrix}, \tag{1}$$

where $\mathbf{r} \triangleq [r_{\mathrm{x}}\ r_{\mathrm{y}}\ r_{\mathrm{z}}]^{\mathrm{T}} \in \mathbb{R}^3$ is the position vector of CM, $\mathbf{f} \triangleq [f_{\mathrm{x}}\ f_{\mathrm{y}}\ f_{\mathrm{z}}]^{\mathrm{T}} \in \mathbb{R}^3$ is the total thrust vector, $m$ is the mass of the vehicle, and $g$ is the gravitational acceleration. As illustrated in Figure 2, $\mathbf{f}$ is perpendicular to the rotor plane.

Define the inclination angle $\phi \in \mathbb{R}$ of the rotor plane as the angle between $Z_{\mathrm{B}}$ and $Z_{\mathrm{R}'}$. The angle $\phi$ can thus be expressed by

$$\phi \triangleq \cos^{-1}\frac{f_{\mathrm{z}}}{f}, \tag{2}$$

where $f \triangleq \|\mathbf{f}\|$.

Define the position tracking error $\tilde{\mathbf{r}} \in \mathbb{R}^3$ as

$$\tilde{\mathbf{r}} \triangleq \mathbf{r} - \mathbf{r}_{\mathrm{d}}, \tag{3}$$

where $\mathbf{r}_{\mathrm{d}} \triangleq [r_{\mathrm{d,x}}\ r_{\mathrm{d,y}}\ r_{\mathrm{d,z}}]^{\mathrm{T}} \in \mathbb{R}^3$ is a position command.

**Problem 1.** Let $\phi_{\max} \in \mathbb{R}$ denote the maximum allowable value of $\phi$, $f_{\min} \in \mathbb{R}$ and $f_{\max} \in \mathbb{R}$ denote, respectively, the minimum and maximum allowable values of $f$, and $\mathbf{r}_{\min} \in \mathbb{R}^3$ and $\mathbf{r}_{\max} \in \mathbb{R}^3$ denote, respectively, the minimum and maximum allowable values of $\mathbf{r}$. The problem is to find a control law for $\mathbf{f}$ that minimizes $\tilde{\mathbf{r}}$, subject to the inclination constraint $\phi \le \phi_{\max}$, to the force magnitude constraint $f_{\min} \le f \le f_{\max}$, and to the position constraint $\mathbf{r}_{\min} \le \mathbf{r} \le \mathbf{r}_{\max}$.

## III. Problem Solution

This section proposes a solution to Problem 1 based on an MPC strategy. Subsection 3.1 describes the system by a discrete-time linear state-space model.

### A. Incremental-Input State-Space Model

Define the state vector $\mathbf{x} \triangleq [r_{\mathrm{x}}\ \dot{r}_{\mathrm{x}}\ r_{\mathrm{y}}\ \dot{r}_{\mathrm{y}}\ r_{\mathrm{z}}\ \dot{r}_{\mathrm{z}}]^{\mathrm{T}} \in \mathbb{R}^6$ and the control input vector $\mathbf{u}\,[u_{\mathrm{x}}\ u_{\mathrm{y}}\ u_{\mathrm{z}}]^{\mathrm{T}} \in \mathbb{R}^3$

$$\mathbf{u} \triangleq \frac{1}{m}\mathbf{f} - \begin{bmatrix} 0 \\ 0 \\ g \end{bmatrix}. \tag{4}$$

Using equation (4), (1) can be immediately rewritten as a continuous-time linear state-space model

$$\dot{\mathbf{x}} = \mathbf{A}\mathbf{x} + \mathbf{B}\mathbf{u}, \tag{5}$$

with

$$\mathbf{A} = \begin{bmatrix} 0 & 1 & 0 & 0 & 0 & 0 \\ 0 & 0 & 0 & 0 & 0 & 0 \\ 0 & 0 & 0 & 1 & 0 & 0 \\ 0 & 0 & 0 & 0 & 0 & 0 \\ 0 & 0 & 0 & 0 & 0 & 1 \\ 0 & 0 & 0 & 0 & 0 & 0 \end{bmatrix} \in \mathbb{R}^{6\times 6} \tag{6}$$

and

$$\mathbf{B} = \begin{bmatrix} 0 & 0 & 0 \\ 1 & 0 & 0 \\ 0 & 0 & 0 \\ 0 & 1 & 0 \\ 0 & 0 & 0 \\ 0 & 0 & 1 \end{bmatrix} \in \mathbb{R}^{6\times 3}. \tag{7}$$

Define the controlled output vector $\mathbf{y} \in \mathbb{R}^3$ to be the position vector, i.e.

$$\mathbf{y} \triangleq \mathbf{C}\mathbf{x}, \tag{8}$$

with

$$\mathbf{C} = \begin{bmatrix} 1 & 0 & 0 & 0 & 0 & 0 \\ 0 & 0 & 1 & 0 & 0 & 0 \\ 0 & 0 & 0 & 0 & 1 & 0 \end{bmatrix} \in \mathbb{R}^{3\times 6}. \tag{9}$$

Let $\mathbf{x}(k) \in \mathbb{R}^6$, $\mathbf{u}(k) \in \mathbb{R}^3$, and $\mathbf{y}(k) \in \mathbb{R}^3$ denote, respectively, the state vector, the control input vector and the controlled output vector, all described in the discrete-time domain. Using the Euler integration method with an integration step of $T_s = 10$ ms, the discretized version of equation (5) and equation (8) is obtained as

$$\begin{array}{rcl} \mathbf{x}(k+1) & = & \mathbf{A}_\mathrm{d}\mathbf{x}(k) + \mathbf{B}_\mathrm{d}\mathbf{u}(k) \\ \mathbf{y}(k) & = & \mathbf{C}_\mathrm{d}\mathbf{x}(k) \end{array}, \tag{10}$$

where

$$\mathbf{A}_\mathrm{d} = \begin{bmatrix} 1 & 0.01 & 0 & 0 & 0 & 0 \\ 0 & 1 & 0 & 0 & 0 & 0 \\ 0 & 0 & 1 & 0.01 & 0 & 0 \\ 0 & 0 & 0 & 1 & 0 & 0 \\ 0 & 0 & 0 & 0 & 1 & 0.01 \\ 0 & 0 & 0 & 0 & 0 & 1 \end{bmatrix} \in \mathbb{R}^{6\times 6}, \tag{11}$$

$$\mathbf{B}_\mathrm{d} = \begin{bmatrix} 0.0001 & 0 & 0 \\ 0.01 & 0 & 0 \\ 0 & 0.0001 & 0 \\ 0 & 0.01 & 0 \\ 0 & 0 & 0.0001 \\ 0 & 0 & 0.01 \end{bmatrix} \in \mathbb{R}^{6\times 3}, \tag{12}$$

and $\mathbf{C}_\mathrm{d} \in \mathbb{R}^{3\times 6}$ remains equal to $\mathbf{C}$.

Consider the discrete-time state-space model of equation (10). It can be rewritten in the incremental-input form as [11]

$$\begin{array}{rcl} \boldsymbol{\xi}(k+1) & = & \tilde{\mathbf{A}}\boldsymbol{\xi}(k) + \tilde{\mathbf{B}}\Delta\mathbf{u}(k) \\ \mathbf{y}(k) & = & \tilde{\mathbf{C}}\boldsymbol{\xi}(k) \end{array}, \tag{13}$$

with

$$\boldsymbol{\xi}(k) = \begin{bmatrix} \Delta\mathbf{x}(k) \\ \mathbf{y}(k) \end{bmatrix} \in \mathbb{R}^9, \tag{14}$$

$$\tilde{\mathbf{A}} = \begin{bmatrix} \mathbf{A}_\mathrm{d} & \mathbf{0}_{6\times 3} \\ \mathbf{C}_\mathrm{d}\mathbf{A}_\mathrm{d} & \mathbf{I}_3 \end{bmatrix} \in \mathbb{R}^{9\times 9}, \tag{15}$$

$$\tilde{\mathbf{B}} = \begin{bmatrix} \mathbf{B}_\mathrm{d} \\ \mathbf{C}_\mathrm{d}\mathbf{B}_\mathrm{d} \end{bmatrix} \in \mathbb{R}^{9\times 3}, \tag{16}$$

and

$$\tilde{\mathbf{C}} = \begin{bmatrix} \mathbf{0}_{3\times 6} & \mathbf{I}_3 \end{bmatrix} \in \mathbb{R}^{3\times 9}, \tag{17}$$

where $\Delta\mathbf{x}(k) \triangleq \mathbf{x}(k) - \mathbf{x}(k-1) \in \mathbb{R}^6$ denotes the incremental state vector, $\Delta\mathbf{u}(k) \triangleq \mathbf{u}(k) - \mathbf{u}(k-1) \in \mathbb{R}^3$ is the incremental control input vector, $\mathbf{I}_3$ represents an identity matrix with dimensions $3\times 3$, and $\mathbf{0}_{3\times 6}$ is a matrix of zeros with dimension $3 \times 6$.

### B. Prediction Model

Using equation (13), the prediction model can be obtained as (see [11], p.50)

$$\hat{\mathbf{y}}_N = \mathbf{G}\Delta\hat{\mathbf{u}}_M + \mathbf{F}, \tag{18}$$

where $\hat{\mathbf{y}}_N$ stacks the controlled outputs along a prediction horizon of length $N$, $\Delta\hat{\mathbf{u}}_M \in \mathbb{R}^{3M\times 1}$ stacks the incremental control inputs along a control horizon of length $M$,

$$\mathbf{G} = \begin{bmatrix} \tilde{\mathbf{C}}\tilde{\mathbf{B}} & \mathbf{0}_{3\times 3} & \dots & \mathbf{0}_{3\times 3} \\ \tilde{\mathbf{C}}\tilde{\mathbf{A}}\tilde{\mathbf{B}} & \tilde{\mathbf{C}}\tilde{\mathbf{B}} & \dots & \mathbf{0}_{3\times 3} \\ \vdots & \vdots & \ddots & \vdots \\ \tilde{\mathbf{C}}\tilde{\mathbf{A}}^{M-1}\tilde{\mathbf{B}} & \tilde{\mathbf{C}}\tilde{\mathbf{A}}^{M-2}\tilde{\mathbf{B}} & \dots & \tilde{\mathbf{C}}\tilde{\mathbf{B}} \\ \vdots & \vdots & & \vdots \\ \tilde{\mathbf{C}}\tilde{\mathbf{A}}^{N-1}\tilde{\mathbf{B}} & \tilde{\mathbf{C}}\tilde{\mathbf{A}}^{N-2}\tilde{\mathbf{B}} & \dots & \tilde{\mathbf{C}}\tilde{\mathbf{A}}^{N-M}\tilde{\mathbf{B}} \end{bmatrix} \in \mathbb{R}^{N\times M} \tag{19}$$

and

$$\mathbf{F} = \begin{bmatrix} \tilde{\mathbf{C}}\tilde{\mathbf{A}} \\ \tilde{\mathbf{C}}\tilde{\mathbf{A}}^2 \\ \vdots \\ \tilde{\mathbf{C}}\tilde{\mathbf{A}}^N \end{bmatrix} \boldsymbol{\xi}(k). \tag{20}$$

### C. Thrust Vector Constraints

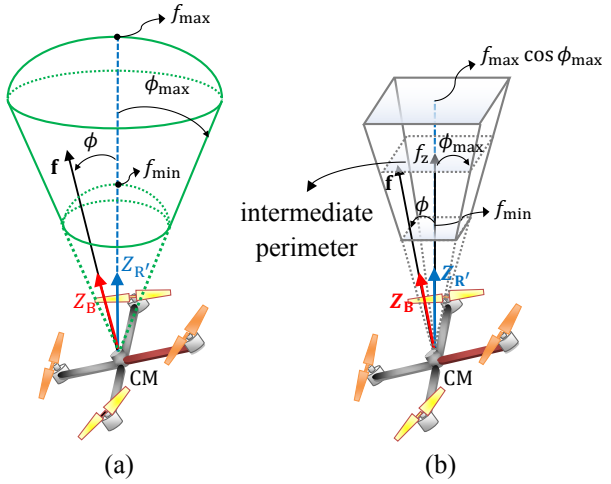


Fig. 3. (a) Original constraint space; (b) Linearized constraint space.

Using equation (4), the thrust magnitude constraint $f_{\min} \le f \le f_{\max}$ can be rewritten in terms of $\mathbf{u}$ as

$$f_{\min} \le \left\| m\mathbf{u} + m\begin{bmatrix} 0 \\ 0 \\ g \end{bmatrix} \right\| \le f_{\max}, \tag{21}$$

or

$$f_{\min} \le m\sqrt{u_\mathrm{x}^2 + u_\mathrm{y}^2 + (u_\mathrm{z} + g)^2} \le f_{\max}. \tag{22}$$

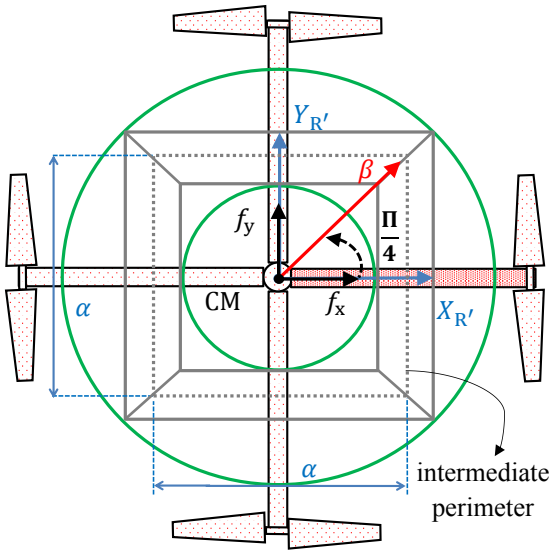


Fig. 4. Top view of the linearized constraint space.

Assuming that $0 \leq \phi_{\max} < \pi/2$ rad, the inclination constraint $\phi \leq \phi_{\max}$ can be replaced by

$$\cos\phi \geq \cos\phi_{\max}. \tag{23}$$

Using equation (2), (23) can be rewritten as

$$\frac{f_z}{f} \geq \cos\phi_{\max}, \tag{24}$$

which in turn, using equation (4), can be rewritten in terms of the components of $\mathbf{u}$, yielding

$$\frac{u_z + g}{\sqrt{u_x^2 + u_y^2 + (u_z + g)^2}} \geq \cos\phi_{\max}. \tag{25}$$

In short, (22) and (25) give the thrust constraints expressed in terms of the components of the control vector $\mathbf{u}$. One can visualize the corresponding constraint space as a conic space with an inferior and a superior spherical lids, as illustrated in Figure 3a. Note that the so-generated constraint space is nonlinear and non-convex.

A linear suboptimal constraint space is now obtained as being a rectangular pyramid inscribed in the original constraint space of Figure 3a. The new constraint space is depicted in Figure 3b.

From Figure 3b, the new constraint along the $Z_{R'}$ axis can immediately be expressed as

$$f_{\min} \leq f_z \leq f_{\max}\cos\phi_{\max}. \tag{26}$$

Consider an arbitrary $f_z$ and let it represent the $Z_{R'}$ axis coordinate of the dotted perimeter depicted in Figure 3b. The projection of this perimeter on the $X_{R'} - Y_{R'}$ plane is depicted in Figure 4. It consists in a square with side $\alpha$ and diagonal $2\beta$. By geometry, one can immediately write

$$\alpha = 2\beta\cos\frac{\pi}{4}, \tag{27}$$

and

$$\beta = f_z\tan\phi_{\max}. \tag{28}$$

Substituting (28) into (27), one obtains

$$\alpha = \sqrt{2}f_z\tan\phi_{\max}. \tag{29}$$

By inspection of Figure 4, one can see that the linear constraints along the $X_{R'}$ and $Y_{R'}$ axes are given by $-\alpha/2 \leq f_x \leq \alpha/2$ and $-\alpha/2 \leq f_y \leq \alpha/2$, respectively. Therefore, from (21), one can finally obtain

$$-\frac{\sqrt{2}}{2}f_z\tan\phi_{\max} \leq f_x \leq \frac{\sqrt{2}}{2}f_z\tan\phi_{\max}, \tag{30}$$

and

$$-\frac{\sqrt{2}}{2}f_z\tan\phi_{\max} \leq f_y \leq \frac{\sqrt{2}}{2}f_z\tan\phi_{\max}. \tag{31}$$

Now, rewriting (26), (30)–(31) in matrix form, yields

$$\mathbf{\Lambda}\,\mathbf{f} \leq \boldsymbol{\lambda}, \tag{32}$$

where

$$\mathbf{\Lambda} = \begin{bmatrix} -1 & 0 & -\frac{\sqrt{2}}{2}\tan\phi_{\max} \\ 1 & 0 & -\frac{\sqrt{2}}{2}\tan\phi_{\max} \\ 0 & -1 & -\frac{\sqrt{2}}{2}\tan\phi_{\max} \\ 0 & 1 & -\frac{\sqrt{2}}{2}\tan\phi_{\max} \\ 0 & 0 & -1 \\ 0 & 0 & 1 \end{bmatrix} \tag{33}$$

and

$$\boldsymbol{\lambda} = \begin{bmatrix} 0 \\ 0 \\ 0 \\ 0 \\ -f_{\min} \\ f_{\max}\cos\phi_{\max} \end{bmatrix}. \tag{34}$$

Finally, using equation (4), (32) can be immediately reformulated in terms of $\mathbf{u}$ as

$$\bar{\mathbf{\Lambda}}\mathbf{u} \leq \bar{\boldsymbol{\lambda}}, \tag{35}$$

where

$$\bar{\mathbf{\Lambda}} \triangleq m\mathbf{\Lambda} \tag{36}$$

and

$$\bar{\boldsymbol{\lambda}} \triangleq \boldsymbol{\lambda} - m\mathbf{\Lambda}\begin{bmatrix} 0 \\ 0 \\ g \end{bmatrix}. \tag{37}$$

Replacing $\mathbf{u}(k) = \Delta\mathbf{u}(k) + \mathbf{u}(k-1)$ in equation (35) and taking it for $M$ instants starting at $k$, the following corresponding constraint equation can be obtained:

$$\mathbf{T}_M\Delta\hat{\mathbf{u}}_M \leq [\bar{\boldsymbol{\lambda}}]_M - \mathrm{diag}(\bar{\mathbf{\Lambda}})[\mathbf{u}(k-1)]_M, \tag{38}$$

where

$$\mathbf{T}_M = \begin{bmatrix} \bar{\mathbf{\Lambda}} & \mathbf{0}_{6\times3} & \cdots & \mathbf{0}_{6\times3} \\ \bar{\mathbf{\Lambda}} & \bar{\mathbf{\Lambda}} & \cdots & \mathbf{0}_{6\times3} \\ \vdots & \vdots & \ddots & \vdots \\ \bar{\mathbf{\Lambda}} & \bar{\mathbf{\Lambda}} & \cdots & \bar{\mathbf{\Lambda}} \end{bmatrix} \in \mathbb{R}^{6M\times3M} \tag{39}$$

is a lower block-triangular matrix, $[\bullet]_M$ is an operator that stacks $M$ copies of a column vector, and $\mathbf{u}(k-1) \in \mathbb{R}^3$ is the control input in the previous discrete-time instant $k-1$.

### D. Constraints on the Controlled Output

Consider the following linear convex inequality constraint for the positions of the multirotor:

$$\mathbf{y}_{\min} \leq \mathbf{y} \leq \mathbf{y}_{\max}. \tag{40}$$

Note that the above constraint can be used to avoid collisions with the bounds of a box-shaped indoor environment. Repeating equation (40) along the prediction horizon, yields

$$[\mathbf{y}_{\min}]_N \leq \hat{\mathbf{y}}_N \leq [\mathbf{y}_{\max}]_N. \tag{41}$$

Replacing the prediction model (18) into equation (41), one can obtain

$$\begin{bmatrix} \mathbf{G} \\ -\mathbf{G} \end{bmatrix} \Delta\hat{\mathbf{u}}_M \leq \begin{bmatrix} [\mathbf{y}_{\max}]_N - \mathbf{F} \\ \mathbf{F} - [\mathbf{y}_{\min}]_N \end{bmatrix}, \tag{42}$$

which consists in the incremental form of the constraints on the controlled output.

### E. Model Predictive Controller

The optimal control vector $\mathbf{u}^*(k)$ computed at the discrete-time instant $k$ is given by $\mathbf{u}^*(k) = \Delta\mathbf{u}^*(k) + \mathbf{u}^*(k-1)$, where $\Delta\mathbf{u}^*(k)$ is the first control vector of $\Delta\mathbf{u}^*_M$, which in turn is obtained by minimizing the following quadratic cost function:

$$J(\Delta\hat{\mathbf{u}}_M) = (\hat{\mathbf{y}}_N - [\mathbf{r}_{\mathrm{d}}]_N)^{\mathrm{T}} \mathbf{Q} (\hat{\mathbf{y}}_N - [\mathbf{r}_{\mathrm{d}}]_N) + \Delta\hat{\mathbf{u}}_M^{\mathrm{T}} \mathbf{R} \Delta\hat{\mathbf{u}}_M, \tag{43}$$

subject to the constraints (38) and (42).

In this work, the controlled output weight $\mathbf{Q}$ and the control input weight $\mathbf{R}$ are chosen as diagonal matrices.

### F. Computing Thrust Magnitude and Attitude Commands

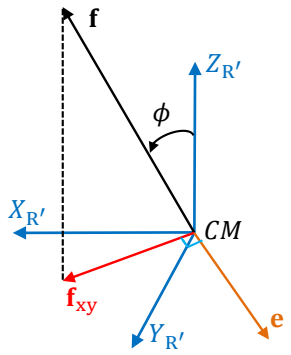


Fig. 5. Relation between the thrust vector $\mathbf{f}$ and its horizontal projection $\mathbf{f}_{\mathrm{xy}}$.

After computation of the control input $\mathbf{u}$, for implementation purposes, it is necessary to transform it into the corresponding commands of total thrust magnitude (throttle) $f$ and attitude.

Rewrite equation (4) as

$$\begin{bmatrix} f_{\mathrm{x}} \\ f_{\mathrm{y}} \\ f_{\mathrm{z}} \end{bmatrix} = m \begin{bmatrix} u_{\mathrm{x}} \\ u_{\mathrm{y}} \\ u_{\mathrm{z}} + g \end{bmatrix}, \tag{44}$$

whose magnitude $f$ is given by

$$f = m\sqrt{u_{\mathrm{x}}^2 + u_{\mathrm{y}}^2 + (u_{\mathrm{z}} + g)^2}, \tag{45}$$

which is the command for the magnitude of the total thrust.

The attitude commands $\mathbf{D}_{\mathrm{d}}$ for the internal attitude control loop (see Figure 1) need to be computed from vector $\mathbf{f}$, which has information about the orientation of the plane of rotors with respect to the local horizontal. Note that there are infinite attitudes of $S_{\mathrm{B}}$ with respect to $S_{\mathrm{R}'}$ for which the $Z_{\mathrm{B}}$ axis coincides with $\mathbf{f}$. In order to specify an unique attitude, it is necessary to select a heading angle. For example (since this work is not concerned with heading control), one can choose a zero heading angle, which is equivalent to just taking into consideration the attitude represented by the principal Euler angle/axis $(\phi, \mathbf{e})$, where $\phi$ is the inclination angle itself and the unit vector $\mathbf{e}$ (see Figure 5) is given by

$$\mathbf{e} = \frac{Z_{\mathrm{R}'} \times \mathbf{f}_{\mathrm{xy}}}{\| Z_{\mathrm{R}'} \times \mathbf{f}_{\mathrm{xy}} \|}, \tag{46}$$

where $\mathbf{f}_{\mathrm{xy}} \triangleq [f_{\mathrm{x}} \ f_{\mathrm{y}}]^{\mathrm{T}}$ denotes the horizontal projection of $\mathbf{f}$. From $(\phi, \mathbf{e})$ one can thus represent the attitude of $S_{\mathrm{B}}$ with respect to $S_{\mathrm{R}}$ using any other attitude parameterization (e.g., quaternion of rotation, modified Rodrigues parameters, Euler angles, and direction cosine matrix) [12].

## IV. Computational Simulations

The 6DOF dynamics of a multirotor is simulated using the Runge-Kutta 4 as the solver with an integration step of 0.001s. The vehicle's mass is $m = 1$ kg and the gravitational acceleration is assumed to be $g = 9.81$ m/s$^2$. In order to solve the optimization problem embedded in the MPC algorithm, the Interior-Point method is taken into account. The following parameterization is adopted for the controller. The control input weights and the controlled output weights are adjusted in $\boldsymbol{\rho} = [0.01 \ 0.01 \ 0.01]^{\mathrm{T}}$ and $\boldsymbol{\mu} = [1 \ 1 \ 1]^{\mathrm{T}}$, respectively. The prediction horizon and control horizon are set to $N = 100$ and $M = 10$, respectively. The maximum and minimum position bounds are $\mathbf{r}_{\max} = [6 \ 6 \ 3]^{\mathrm{T}}$ and $\mathbf{r}_{\min} = [0 \ 0 \ 0]^{\mathrm{T}}$, respectively. The maximum and minimum constraints on the force magnitude are set in $f_{\max} = 20$ N and $f_{\min} = 2$ N, respectively. The attitude controller are proportional-derivative laws tuned so as to make the attitude dynamics have a bandwidth significantly larger than the bandwidth of the position control dynamics.

The position commands chosen for evaluation of the method are trajectories composed by a set of straight lines from the initial position $\mathbf{r}_i = [1 \ 1 \ 0]^{\mathrm{T}}$ to the final position $\mathbf{r}_f = [5 \ 5 \ 1]^{\mathrm{T}}$ passing by the waypoints $\mathbf{w}_1 = [1 \ 1 \ 1]^{\mathrm{T}}$, $\mathbf{w}_2 = [2 \ 2 \ 2]^{\mathrm{T}}$, $\mathbf{w}_3 = [4 \ 2 \ 2]^{\mathrm{T}}$, $\mathbf{w}_4 = [5 \ 3 \ 2]^{\mathrm{T}}$, $\mathbf{w}_5 = [5 \ 5 \ 2]^{\mathrm{T}}$. Three different speed values are considered: $v = 0.5$ m/s, $v = 1.0$ m/s, and $v = 2.0$ m/s. Nine Monte-

TABLE I
MONTE-CARLO SIMULATION RESULTS FOR DIFFERENT VALUES OF $v$ AND $\phi_{\max}$.

| $v$ m/s | $\phi_{\max}$ deg | $e_x$ m | $e_y$ m | $e_z$ m | $I_x$ % | $I_y$ % | $I_z$ % | $I_\phi$ % | $I_{\text{fmax}}$ % | $I_{\text{fmix}}$ % |
|---|---|---|---|---|---|---|---|---|---|---|
| 0.5 | 10 | 0.087 | 0.087 | 0.065 | 0.00 | 0.00 | 0.00 | 1.39 | 0.00 | 0.00 |
| | 20 | 0.075 | 0.075 | 0.065 | 0.00 | 0.00 | 0.00 | 0.00 | 0.00 | 0.00 |
| | 30 | 0.075 | 0.074 | 0.065 | 0.00 | 0.00 | 0.00 | 0.00 | 0.00 | 0.00 |
| 1.0 | 10 | 0.190 | 0.234 | 0.136 | 0.00 | 0.00 | 0.00 | 6.49 | 0.12 | 0.00 |
| | 20 | 0.137 | 0.135 | 0.115 | 0.00 | 0.00 | 0.00 | 0.00 | 0.00 | 0.00 |
| | 30 | 0.135 | 0.132 | 0.113 | 0.00 | 0.00 | 0.00 | 0.00 | 0.00 | 0.00 |
| 2.0 | 10 | 0.592 | 0.582 | 0.338 | 2.10 | 2.10 | 2.11 | 28.53 | 3.51 | 0.61 |
| | 20 | 0.289 | 0.306 | 0.187 | 0.00 | 0.00 | 0.00 | 5.44 | 0.00 | 0.00 |
| | 30 | 0.235 | 0.231 | 0.190 | 0.00 | 0.00 | 0.00 | 1.12 | 0.00 | 0.00 |

Carlo simulations of 20 runs are carried out, considering in each case a different combination of speed $v$ and maximum inclination constraint $\phi_{\max}$.

The following figure of merit is used to evaluate the position control error:

$$e_q \triangleq \frac{1}{N\sqrt{k_f}} \sum_{i=1}^{N} \sqrt{\sum_{k=1}^{k_f} \left( r_{d,q}(k) - r_q^{(i)}(k) \right)^2}, \qquad (47)$$

for $q$ equal to $x$, $y$, $z$; $r_q^{(i)}(k)$ denotes the $i$-th realization of $r_q(k)$. For evaluating the frequency of constraint violation, the following figure of merit is adopted:

$$I_l \triangleq \frac{1}{Nk_f} \sum_{i=1}^{N} M_l^{(i)}, \qquad (48)$$

where $M_l^{(i)}$ is the number of discrete time instants (of the $i$-th realization) in which the $l$ constraint is violated, for $l$ equal to $x$, $y$, $z$, $\phi$, $f_{\min}$, $f_{\max}$.

The simulation results are summarized in Table 1. First, one can observe that the control error increases as the speed of the trajectory is increased or as the maximum inclination constraint is decreased. For example, for $v = 0.5$ m/s, position errors stay below 9 cm, whereas they approach 60 cm when the speed is set to $v = 2.0$ m/s. Still concerning the position error, one can see smaller errors along the $Z_R$ axis. Regarding the violation of position constraints, no occurrence are observed with the two smaller speeds, $v = 0.5$ m/s and $v = 1.0$ m/s. Concerning the maximum inclination constraint, for all speed values, the number of violations reduces as $\phi_{\max}$ is increased. Finally, the frequency of violations of $f_{\min}$ and $f_{\max}$ increases as the speed of the trajectory is increased, but decreases as $\phi_{\max}$ is increased.

## V. CONCLUSIONS

This paper tackled the problem of controlling the position of a multirotor helicopter subject to constraints on the inclination of the rotor plane, on the total thrust magnitude, and on the position of the vehicle. The problem was solved using a simple linear-quadratic state-space MPC formulation, which became possible thanks to the replacement of an original conic constraint space on the total thrust vector by an inscribed rectangular pyramid. The method was evaluated by computational simulations considering that the vehicle was subject to a Gaussian disturbance force. One can conclude that the proposed method is able to control the multirotor position, even under disturbance forces, while respecting the position and control constraints. However, if a rapid position command is required, it is necessary to relax the maximum inclination constraint in order to have sufficient lateral control accelerations to overcome the disturbance forces. In summary, the proposed method, if adequately used, can be a good solution for the position control of multirotors in indoor environments and urban areas. For a future work, a flight test environment is being prepared for experimental evaluation of the proposed method.

## ACKNOWLEDGMENT

The authors would like to thank FAPEAM/Brazil by research grants 028/2011 and the Instituto Tecnológico de Aeronáutica by the necessary support to realize the present work.

## REFERENCES

[1] G. M. Hoffman, S. L. Waslander, C. J. Tomlin. Quadrotor Helicopter Trajectory Tracking Control, *Proceedings of the AIAA Guidance, Navigation and Control Conference and Exhibit*, Honolulu, Hawaii, 2008.

[2] K. Alexis, C. Papachristos, G. Nikolakopoulos, A. Tzes. Model predictive quadrotor indoor position control, *Proceedings of the 19th Mediterranean Conference on Control and Automation*, Corfu, Greece, 2011.

[3] V. Mistler, A, Benallegue, N. K. M'Sirdi. Exact linearization and noninteracting control of a 4 rotors helicopter via dynamic feedback, *Proceedings of the 2001 IEEE International Workshop on Robot and Human Interactive Communication*, Corfu, Greece, 2011, 29-39.

[4] P. Castillo, A. Dzul, R. Lozano. Real-Time stabilization and tracking of a four-rotor mini rotorcraft, *IEEE Transaction on Control Systems Technology*, 2004, 510-516.

[5] S. Bouabdallar, R. Siewart. Backstepping and Sliding-mode Technique Applied to an Indoor Micro Quadrotor, *Proceedings of the 2005 IEEE International Conference on Robotics and Automation*, Barcelona, Spain, 2005.

[6] G. V. Raffo, M. G. Ortega, F. R. Rubio. An integral predictive/nonlinear $\mathcal{H}_\infty$ control structure for a quadrotor helicopter , *Automatica*, Vol. 46, 29-39.

[7] R. V. Lopes, P. H. R. Q. A. Santana, G. A. Borgues, J. Y. Ishihara. Model predictive control applied to tracking and attitude stabilization of a vtol quadrotor aircraft, *Proceedings of the 21st International Congress of Mechanical Engineering*, Natal, Brasil, 2011.

[8] I. A. A. Prado, D. A. Santos. Multirotor position tracking using a linear constrained model predictive controller, *22nd International Congress of Mechanical Engineering*, Ribeiro Preto, SP, 2013.

[9] D. A. Santos, O. Saotome, A. Cela. Trajectory control of multirotor helicopters with thrust vector constraints. In: 2013 21st Mediterranean Conference on Control & Automation (MED), 2013, Platanias. 21st Mediterranean Conference on Control and Automation, 2013. p. 375.

[10] J. Yan, D. A. Santos, D. S. Bernstein. Adaptive Control with Convex Saturation Constraints. In: Dynamic Systems and Control Conference, 2013, Palo Alto. Proceedings of the ASME 2013 Dynamic Systems and Control Conference, 2013.

[11] J. M. Maciejowski. Predictive Control with Constraints. Harlow: Prentice-Hall, 2002.

[12] M. Shuster, A Survey of Attitude Representations, *The Journal of the Astronautical Sciences*, 41(4), 1993, 439-517.